Chinese Journal of Chemical Engineering 85 (2025) 270–279

Contents lists available at ScienceDirect

Chinese Journal of Chemical Engineering

journal homepage: www.elsevier.com/locate/CJChE

Full Length Article

Selective catalytic deoxygenation of 1-octanol from Fischer-Tropsch C10 mixed oil

Yongbin Shen [1,2], Qihe Ma [3], Hua Yuan [2], Chuang Liu [3], Likun Yang [2], Hao Huang [2], Bowen Shi [2], Zhenhua Li [1], Shunyu Liang [3], Hu Li [2,*], Zhengping Dong [3,*]

[1] School of Chemical Engineering and Technology, Tianjin University, Tianjin 300072, China
[2] Ningxia Coal Industry Co., LTD, China Energy Investment, Yinchuan 750011, China
[3] College of Chemistry and Chemical Engineering, Lanzhou University, Lanzhou 730000, China

ARTICLE INFO

Article history:
Received 20 February 2025
Received in revised form
7 April 2025
Accepted 11 April 2025
Available online 13 May 2025

Keywords:
Alumina
Fixed-bed
Reaction kinetics
Catalytic deoxygenation
Fischer-Tropsch oil

ABSTRACT

The selective catalytic deoxygenation of oxy-organics in Fischer-Tropsch mixed oil for its high value utilization is challenging. Herein, a $BaCO_3/\gamma$-Al_2O_3 catalyst was prepared calcining γ-Al_2O_3 with $BaCO_3$, and the acid-alkalinity of the catalyst was regulated by introducing alkaline Ba basic sties. In a continuous fixed-bed reactor with a feed mass space velocity of 1 h^{-1} and reaction temperature of 330 °C, $BaCO_3/\gamma$-Al_2O_3 catalyst can efficiently catalyzed the deoxygenation removal of 1-octanol in Fischer-Tropsch C10 mixture oil. It also inhibited the isomerization of 1-decene in the C10 mixture. The catalytic deoxygenation kinetics of 1-octanol were also studied. The reaction was endothermic with an activation energy of 64 kJ·mol^{-1} and a reaction order of 2. In addition, theoretical studies revealed the adsorption and activation of 1-decene on the Lewis acidic site and the alkaline Ba basic sites, 1-decene was more easily underwent isomerization into 2-decene at Lewis acid sites. This research provides a useful method to enable the industrial application of catalytic deoxygenation of alcohols in Fischer-Tropsch synthetic oil.
© 2025 The Chemical Industry and Engineering Society of China, and Chemical Industry Press Co., Ltd. All rights are reserved, including those for text and data mining, AI training, and similar technologies.

1. Introduction

Fischer-Tropsch synthesis is used to produce liquid fuels and oil products to replace petroleum-based gasoline, diesel, and lubricating oil [1–3]. High-temperature Fischer-Tropsch synthesis mainly produces liquid oil products that contain 50% to 60% olefins, most of which are α-olefins [4]. α-Olefins are important chemical raw materials that can be copolymerized with ethylene or used to synthesize detergents and lubricants [5,6]. However, long-chain α-olefins are mostly derived from ethylene polymerization, which requires a high energy consumption and products with complex compositions [7]. α-Olefins can be separated from high-temperature Fischer-Tropsch synthetic oil [8], but the existence of oxygen-containing organic compounds such as alcohols, ketones, and acids in high-temperature Fischer-Tropsch synthetic oil restricts the further applications of α-olefin. Of these, alcohols account for more than 90% of the total amount of oxygen-containing compounds [9], and if they are not removed before subsequent processing of Fischer-Tropsch synthetic oil, they may corrode equipment or poison catalysts during conversion processes [10]. Therefore, the removal of alcohols is important for further practical applications of Fischer-Tropsch synthetic oil.

Distillation, adsorption, and selective hydrogenation are commonly used for the desulfurization and deoxygenation of Fischer-Tropsch synthetic oil [11]. However, distillation requires large investments and energy consumption, and it is difficult to deeply remove alcohols. The capacity of adsorbents is small and they must be regenerated several times [12]. Selective hydrogenation requires the use of hydrogen to remove oxygen-containing compounds, and olefins are easily hydrogenated to saturated alkanes, which reduces the utilization value of synthetic oil [13]. In contrast, catalytic deoxygenation of alcohols in Fischer-Tropsch synthetic oil uses simple reaction conditions, provides good selectivity, and can convert olefins while removing oxygen-containing organic compounds [14]. In recent years, the catalytic dehydration of alcohols in Fischer-Tropsch synthetic oil has attracted much attention [15–17]. Previous studies have found that ideal products of alcohol dehydration such as olefins and ethers are formed at the acidic sites of the catalyst [18,19], while aldehydes and ketones are formed at the alkaline sites [20,21]. Therefore, in alcohol-catalyzed deoxygenation processes with multiple steps, acidic catalysts are often required to split C—O bonds [22]. Thus, it

* Corresponding authors.
E-mail addresses: 15010874@ceic.com (H. Li), dongzhp@lzu.edu.cn (Z. Dong).

https://doi.org/10.1016/j.cjche.2025.04.009
1004-9541/© 2025 The Chemical Industry and Engineering Society of China, and Chemical Industry Press Co., Ltd. All rights are reserved, including those for text and data mining, AI training, and similar technologies.

is important to develop efficient catalysts for the catalytic dehydration of alcohols in Fischer-Tropsch synthetic oil.

The catalytic dehydration of alcohols on the surface of solid acidic catalysts mainly involves an acid-base center synergistic reaction mechanism [23,24]. C—O bond cracking reaction on C—OH occurs at the acidic sites, and β-H bonds are captured at the alkaline sites, and the resulting β fracture forms water and olefin. The alcohols produced by high-temperature Fischer-Tropsch synthesis are mainly primary alcohols that can in principle react to form α-olefins and increase the reserve of useful α-olefins. However, in the presence of an acidic catalyst, a considerable portion of α-olefins in Fischer-Tropsch synthetic oil at high temperatures will isomerize into internal olefins, which is unfavorable to increasing the yield of α-olefins [25,26]. Solid acid catalysts also lead to the cracking and polymerization of alkanes and olefins, which will further reduce the added value of Fischer-Tropsch synthetic oil [27,28]. Therefore, it is important to design and develop high-performance catalysts for the selective dehydration of alcohols while prevent the isomerization of α-olefins in Fischer-Tropsch synthetic oil.

Based on the aforementioned considerations, this research is dedicated to the development of highly efficient catalytic systems for the deoxygenation refining of Fischer-Tropsch synthetic oil, with a specific focus on mitigating the isomerization of α-olefins. Through precise acid-base modulation, a series of $BaCO_3$-modified γ-Al_2O_3 catalysts were meticulously engineered and prepared. These catalysts successfully facilitated the catalytic dehydration of alcohols present in Fischer-Tropsch synthetic oil, thereby yielding α-olefins while concurrently suppressing the isomerization of pre-existing α-olefins. Furthermore, this study elucidated the underlying mechanisms governing α-olefin isomerization during the catalytic dehydration of alcohols, thereby establishing a robust theoretical framework that supports the industrial-scale implementation of alcohol catalytic deoxygenation in Fischer-Tropsch synthetic oil refining processes.

2. Materials and Methods

2.1. Materials and reagents

The pseudo-boehmite powder was purchased from Shanghai Titan Science and Technology Co., Ltd. $BaCO_3$ and concentrated HNO_3 were purchased from Shanghai Macklin Biochemical Co., Ltd. The high-temperature Fischer-Tropsch synthetic oil C10 distillate was provided by Ningxia Coal Industry Co., Ltd. Other reagents required for this study were commercially available and used without purification before use.

2.2. Preparation of catalyst

1%$BaCO_3$/γ-Al_2O_3 catalyst was prepared as follows: 50 g of pseudo-boehmite powder was added to a 100 ml beaker, followed by 0.5 g $BaCO_3$. 3 mol·L^{-1} HNO_3 was slowly added, and the mixture was stirred with a glass stirring rod. When the mixture was semi-dry, it was squeezed with an extruder to form rod-like samples with a diameter of 1 mm. The rod-like samples were dried and roasted at 600 °C for 5 h, and then 1%$BaCO_3$/γ-Al_2O_3 catalyst was obtained. 2%$BaCO_3$/γ-Al_2O_3 and 3%$BaCO_3$/γ-Al_2O_3 catalysts were prepared by a similar method.

2.3. Catalytic deoxygenation of 1-octanol from Fischer-Tropsch C10 mixed oil

A continuous fixed-bed reactor was used to evaluate the catalytic deoxygenation of 1-octanol from Fischer-Tropsch C10 mixed oil under normal pressure. Typically, 4.6 g 1%$BaCO_3$/γ-Al_2O_3 catalyst was loaded into the fixed-bed reactor, and the temperature program was set to 10 °C·min^{-1}, from room temperature to 290 °C. The C10 mixture was fed into the reactor through a plunger pump for catalytic deoxygenation. The C10 oil was composed of 56.3% 1-decene, 19.63% decane, 6.14% isodecene, and 1.4% 1-octanol. The catalytic deoxygenation reaction was performed at 290, 300, 310, 320 and 330 °C, and the injection rate of the C10 mixture oil was adjusted to 100 μl·min^{-1}, 150 μl·min^{-1}, and 200 μl·min^{-1}, respectively. Catalytic deoxygenation using 2%$BaCO_3$/γ-Al_2O_3 and 3%$BaCO_3$/γ-Al_2O_3 was evaluated using a similar method.

2.4. Characterization

The microstructure and morphology of the catalysts were investigated by scanning electron microscopy (SEM, Apreo S) and transmission electron microscopy (TEM, FEI Talos 200s). The crystallographic properties of the catalysts were characterized by powder X-ray diffraction (PXRD, Rigaku MiniFlex 600), and data were recorded in the 2θ range of 10°—90° with Cu-K_α radiation. Information about chemical bonds was acquired with Fourier-transform infrared spectroscopy (FT-IR, Nicolet NEXUS 670) using KBr pellets. Nitrogen adsorption-desorption isotherms were obtained at −196 °C on a Micromeritics ASAP 2460 instrument, and the Brunauer-Emmett-Teller (BET) method was used to obtain the specific surface areas. The non-local density functional theory (NLDFT) model was employed to analyze the pore size distributions.

2.5. Computational methods

The mechanism of intrinsic migration of 1-decene terminal double bonds was evaluated by using the Vienna Ab-initio Simulation Package (VASP) [29,30]. During geometric optimization, a vacuum layer of 2 nm was used to avoid interactions between adjacent plates. The generalized gradient approximation (GGA) of the Perdew-Burke-Ernzerhof (PBE) functional was used to describe electron exchange and correlation effects [31]. The Kohn-Sham equation was expanded using a plane wave base set with a cutoff energy of 400 eV. The Brillouin region was sampled by a 2 × 2 × 1 Gamma *k* grid. The geometric optimization converged to the point where the force acting on each atom was less than 0.5 eV·nm^{-1} and the total energy was less than 10^{-5} eV.

3. Results and Discussion

3.1. Characterization of catalysts

The crystal structures of γ-Al_2O_3 and $BaCO_3$/γ-Al_2O_3 catalysts were investigated by PXRD. As shown in Fig. 1, the PXRD pattern of Al_2O_3 was in good agreement with the PXRD pattern of γ-Al_2O_3 (PDF:29-0063) [32], and the lattice planes of γ-Al_2O_3 (2 2 2), (4 0 0), and (4 4 0) were present. When a very small amount of $BaCO_3$ was loaded on γ-Al_2O_3 and then calcined, the resulting Ba species had a small size, resulting in PXRD only showing the characteristic peaks of γ-Al_2O_3. The uniform dispersion of Ba species on γ-Al_2O_3 could be further proved by the following element mapping. This indicates that the $BaCO_3$/γ-Al_2O_3 catalysts were successfully prepared. The uniform dispersion of alkaline Ba species masked the acidic sites on the surface of γ-Al_2O_3, which helped maintain α-olefins in C10 distillate during the catalytic deoxygenation of alcohols process and prevent their isomerization.

The nitrogen adsorption-desorption isotherms of γ-Al_2O_3 and $BaCO_3$/γ-Al_2O_3 catalysts in Fig. 2(a) are type IV isotherms. This indicates that the catalysts contained abundant mesopores [33], which can promote adsorption and mass transfer during catalytic

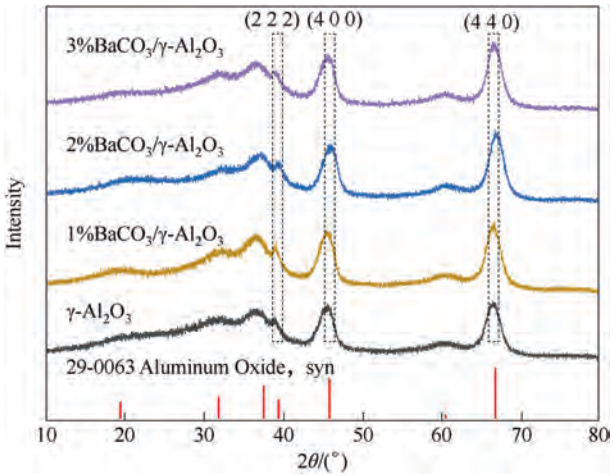

Fig. 1. PXRD patterns of γ-Al_2O_3 and $BaCO_3$/γ-Al_2O_3 catalysts.

reactions. The specific surface area of γ-Al_2O_3 was 202.7 $m^2 \cdot g^{-1}$. After modification by the adsorptive loading of $BaCO_3$, the specific surface areas of 1%$BaCO_3$/γ-Al_2O_3, 2%$BaCO_3$/γ-Al_2O_3, and 3%$BaCO_3$/γ-Al_2O_3 decreased to 198.6 $m^2 \cdot g^{-1}$, 193.2 $m^2 \cdot g^{-1}$, and 191.1 $m^2 \cdot g^{-1}$, respectively, and the pore volumes of γ-Al_2O_3, 1%$BaCO_3$/γ-Al_2O_3, 2%$BaCO_3$/γ-Al_2O_3, and 3%$BaCO_3$/γ-Al_2O_3 were 0.62, 0.57, 0.55 and 0.54 $cm^3 \cdot g^{-1}$ respectively, indicating that adsorption and calcining with $BaCO_3$ partially covered and blocked micropores. The average pore sizes of γ-Al_2O_3, 1%$BaCO_3$/γ-Al_2O_3, 2%$BaCO_3$/γ-Al_2O_3, and 3% $BaCO_3$/γ-Al_2O_3 were 12.4, 11.8, 11.7 and 11.4 nm, respectively (Fig. 2b). The SEM images of γ-Al_2O_3 and $BaCO_3$/γ-Al_2O_3 catalysts in Fig. 3(a)–(d) show their amorphous powder structure, which was porous and loose [34]. Fig. 3(e)–(h) show the high-resolution TEM images of the prepared γ-Al_2O_3 and $BaCO_3$/γ-Al_2O_3 catalysts. The microstructure of the γ-Al_2O_3 powder presented a rod-like and granular packing structure with a loose porous packing mode. After adsorption with 1% to 3% of $BaCO_3$ and high-temperature roasting, the structure of the γ-Al_2O_3 powder remained intact, with a porous and loose structure, which should promote reactants diffusion, mass transfer, and heat transfer during reactions. TEM analysis revealed that compared with γ-Al_2O_3, no Ba species were observed in 1%$BaCO_3$/γ-Al_2O_3, 2%$BaCO_3$/γ-Al_2O_3, and 3%$BaCO_3$/γ-Al_2O_3. This might be attributed to the low loading amount or the porous and loose structure of γ-Al_2O_3, which led to the uniform dispersion of Ba species. This result was consistent with the XRD results (Fig. 1). The TEM element mapping of 3%$BaCO_3$/γ-Al_2O_3 show that Al, O, Ba and other species were uniformly distributed over the catalyst, and the high dispersion of Ba species masked the surface acid sites of γ-Al_2O_3 (Fig. 3(i)).

The FT-IR spectra of $BaCO_3$/γ-Al_2O_3 catalysts are shown in Fig. S1. The absorption vibration peak around 3500 cm^{-1} was mainly the –OH vibration peak on the surface of the γ-Al_2O_3 material [35]. The infrared absorption peak in the range of 400–1000 cm^{-1} is the vibration absorption peak of Al—O bond [36]. The infrared absorption peak of about 1600–1700 cm^{-1} may be the characteristic absorption peak of CO_2 adsorbed on the surface of γ-Al_2O_3. With the increase of $BaCO_3$ loading amount, the infrared absorption peak of 1450 cm^{-1} gradually decreases.

Fig. 4 shows the pyridine-adsorbed FT-IR spectra of a series of $BaCO_3$/γ-Al_2O_3 catalysts (the detail method for the pyridine-adsorbed FT-IR analysis was provided in the Supplementary Material). The infrared absorption peak of γ-Al_2O_3 appeared at 1450 cm^{-1}, indicating that it contained Lewis acid sites. After calcining with $BaCO_3$, the peak at 1450 cm^{-1} disappeared upon increasing the loading of $BaCO_3$, indicating that the Lewis acid sites in γ-Al_2O_3 were covered by basic BaO sites. The pyridine peak of 1% $BaCO_3$/γ-Al_2O_3 disappeared at 200 °C, that of 2%$BaCO_3$/γ-Al_2O_3 disappeared at 150 °C, and that of 3%$BaCO_3$/γ-Al_2O_3 disappeared at 100 °C. With the increase of $BaCO_3$ loading, the desorption temperature gradually decreased, indicating that the acidity gradually weakened. When the loading of $BaCO_3$ reached 3%, the peak at 1450 cm^{-1} almost disappeared. Because the Lewis acid sites easily catalyzed the isomerization of α-olefins, the Lewis acid sites of $BaCO_3$/γ-Al_2O_3 after being neutralized by the Ba base sites greatly decreased. This will promote the catalysis of the dehydration of 1-octanol in C10 Fischer-Tropsch synthetic oil, which may prevent the isomerization loss of 1-decene.

3.2. Catalytic deoxygenation of Fischer-Tropsch C10 mixed oil

γ-Al_2O_3 was loaded with 1% (mass) $BaCO_3$ and calcined at 600 °C to obtain 1%$BaCO_3$/γ-Al_2O_3 catalyst. The fixed-bed reactor equipped with 4.6 g 1%$BaCO_3$/γ-Al_2O_3 was heated to 290 °C. The injection rate of C10 mixed oil was 100 $\mu l \cdot min^{-1}$, and the mass airspeed was 1 h^{-1}. Fig. 5(a) shows that at 290 °C, the isomerization ratio of 1-decene in C10 mixed oil was higher during the initial reaction stage, and the isomerization loss ratio of 1-decene gradually decreased from 14.96% to 0.3% upon extending the reaction time.

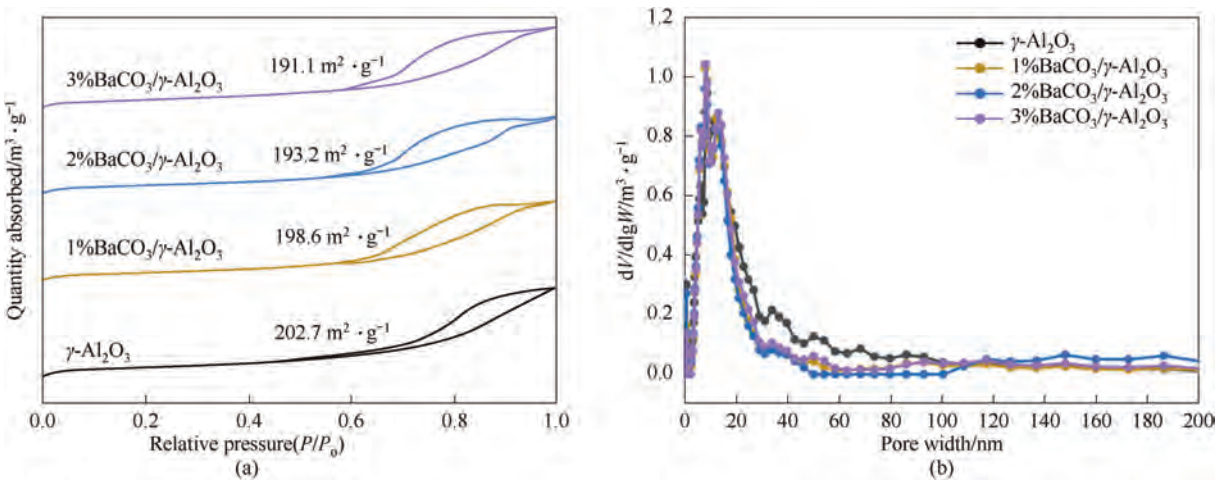

Fig. 2. (a) Nitrogen adsorption-desorption isotherms of γ-Al_2O_3 and $BaCO_3$/γ-Al_2O_3 catalysts. (b) The corresponding pore size distribution curves of γ-Al_2O_3 and $BaCO_3$/γ-Al_2O_3 catalysts.

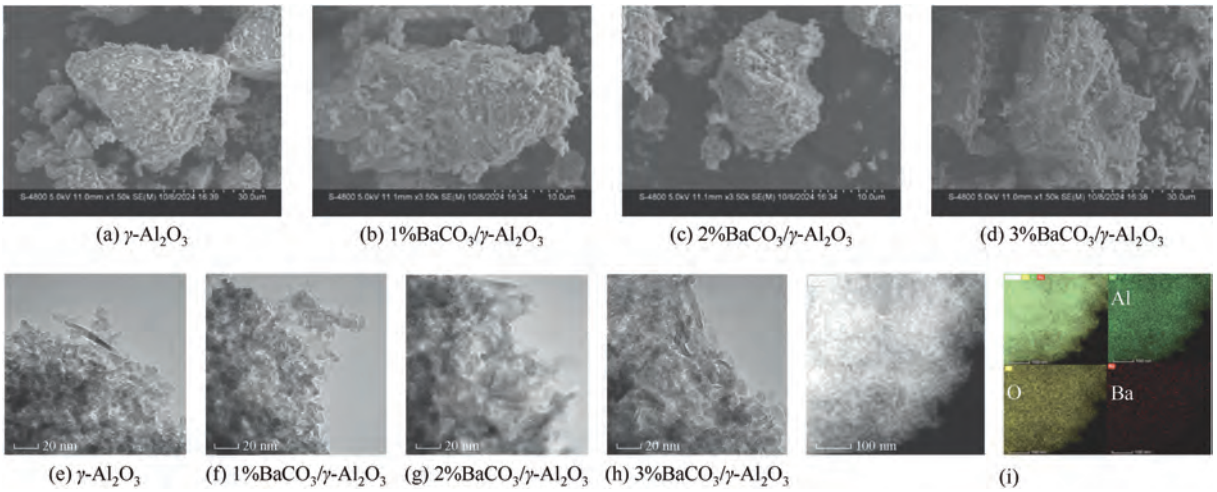

Fig. 3. SEM images of γ-Al_2O_3 (a), 1%$BaCO_3$/γ-Al_2O_3 (b), 2%$BaCO_3$/γ-Al_2O_3 (c), 3%$BaCO_3$/γ-Al_2O_3 (d); TEM images of γ-Al_2O_3 (e), 1%$BaCO_3$/γ-Al_2O_3 (f), 2%$BaCO_3$/γ-Al_2O_3 (g), and 3% $BaCO_3$/γ-Al_2O_3 (h); Element mapping images of 3%$BaCO_3$/γ-Al_2O_3 (i).

However, at 290 °C, the deoxygenation conversion of 1-octanol was lower (<85%). The reaction temperature of the fixed-bed reactor was increased to 300 °C, and the injection rate was maintained at 100 $\mu l \cdot min^{-1}$. The isomerization ratio of 1-decene was about 0.6%, and the dehydration conversion rate of 1-octanol was 86% to 89%. When the reaction temperature was further increased to 310 °C, 320 °C, and 330 °C, the average loss of 1-decene gradually increased to an average of 0.8%, 0.9%, and 1.4%, respectively. The dehydration conversion of 1-octanol gradually increased to an average of 89%, 94%, and 97%, respectively (Fig. 5(b)). The results show that the

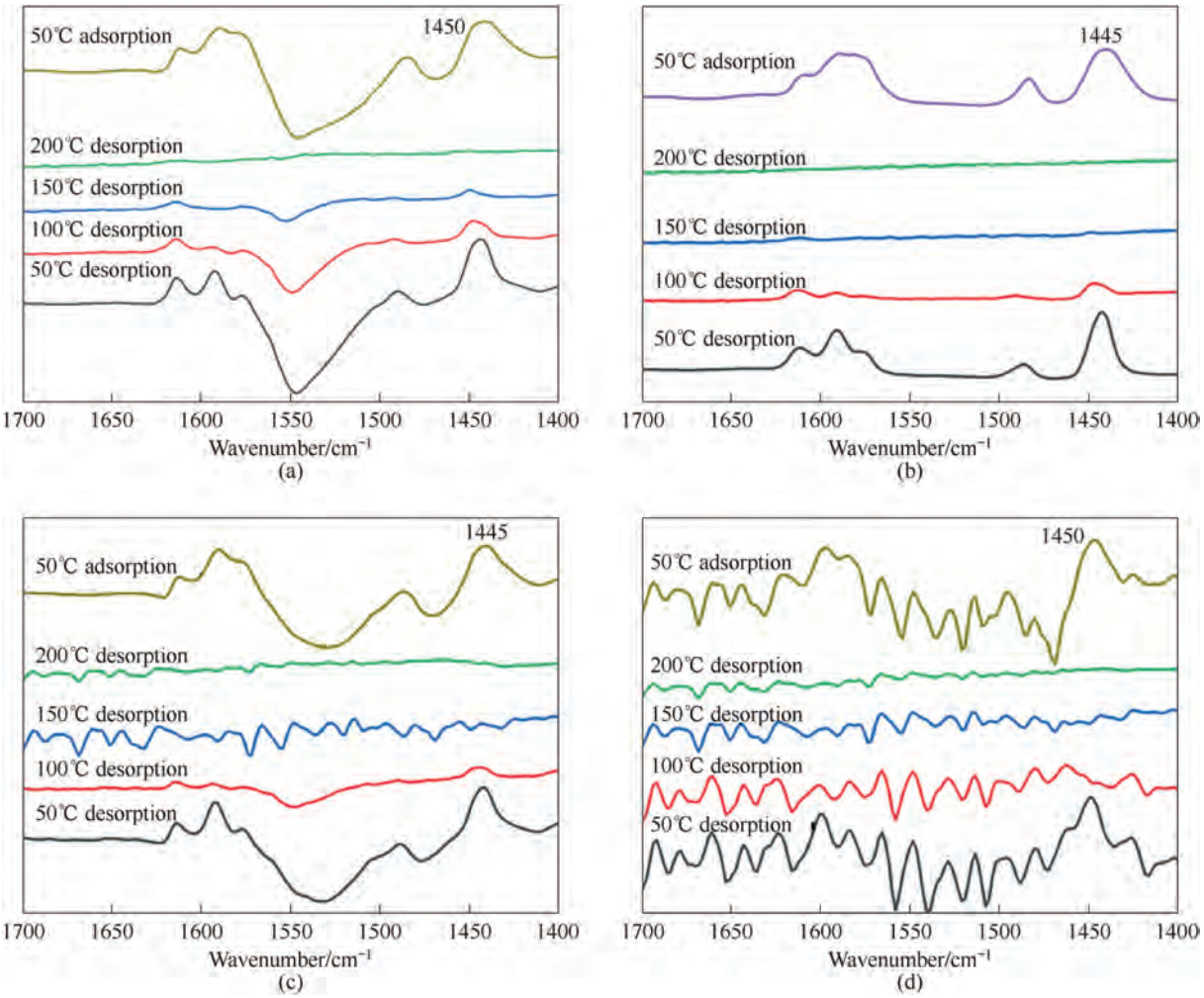

Fig. 4. Pyridine-adsorbed FT-IR spectra results of γ-Al_2O_3 (a), 1%$BaCO_3$/γ-Al_2O_3 (b), 2%$BaCO_3$/γ-Al_2O_3 (c) and 3%$BaCO_3$/γ-Al_2O_3 (d).

dehydration ratio of 1-octanol increased gradually with the increase of reaction temperature [37,38], but 1-decene tended to isomerize into an internal olefin at higher temperatures. At 330 °C, the injection rate of C10 mixed oil was adjusted to 100 μl·min^{-1}, 150 μl·min^{-1}, and 200 μl·min^{-1}, respectively. Fig. 5(c) shows the isomerization loss ratio of 1-decene at different injection rates, which was stable at less than 1.5%. As shown in Fig. 5(d), at a reaction temperature of 330 °C, the catalytic dehydration ratio of 1-octanol significantly decreased upon increasing the injection rate. When only 100 μl·min^{-1} was injected and the mass airspeed was 1 h^{-1}, the removal conversion rate of 1-octanol exceeded 96%.

The dehydration performance of 2%$BaCO_3$/γ-Al_2O_3 catalyst was evaluated using an evaluation method similar to the one mentioned above. Fig. 6(a) shows that the reaction effect was similar to that of 1%$BaCO_3$/γ-Al_2O_3 catalyst, *i.e.*, during the initial reaction stage, the isomerization rate of 1-decene was high, and upon extending the reaction time, the isomerization loss rate of 1-decene gradually decreased from 11% to 0.7%. However, at 290 °C, the dehydration conversion of 1-octanol was between 75% and 80%. When the reaction temperature of the fixed bed was increased to 300, 310, 320 and 330 °C. The isomerization ratio of 1-decene gradually increased to 1.6%, and the dehydration ratio of 1-octanol increased to 85%, 91%, 94%, and 97% (Fig. 6(b)). The results showed that the higher reaction temperature promoted the removal of 1-octanol. Similar to the reaction effect of 1%$BaCO_3$/γ-Al_2O_3 catalyst, the injection rate of C10 mixed oil was adjusted to 100, 150 and 200 μl·min^{-1}, respectively, at 330 °C. Fig. 6(c) shows the isomerization loss ratio of 1-decene at different injection rates, which remained stable below 1.5%. Fig. 6(d) shows that at a reaction temperature of 330 °C, the catalytic removal rate of 1-octanol at different injection rates significantly decreased upon increasing the injection rate. When 100 μl·min^{-1} was injected and the mass airspeed was 1 h^{-1}, the removal of 1-octanol reached approximately 97%.

The dehydration performance evaluation of C10 mixed oil catalyzed by 3%$BaCO_3$/γ-Al_2O_3 catalyst is shown in Table 1. At a reaction temperature of 290 °C, the isomerization ratio of 1-decene was high during the initial reaction stage, and the isomerization loss ratio of 1-decene gradually decreased from 7.8% to below 1% upon extending the reaction time. However, at a reaction temperature of 290 °C, the dehydration conversion of 1-octanol was about 90%. When the reaction temperature of the fixed-bed reactor was increased to 310 °C and 330 °C, the isomerization ratio of 1-decene remained at about 1% in both cases, and the removal rate of 1-octanol increased to 97% and 99%, respectively. These results show that 3%$BaCO_3$/γ-Al_2O_3 catalyzed the dehydration of 1-octanol at 310 °C. These results show that the 3%$BaCO_3$/γ-Al_2O_3 catalyst has the best catalytic dehydration and inhibition of 1-decene isomerization performance in Fischer-Tropsch C10 mixed oil [39,40].

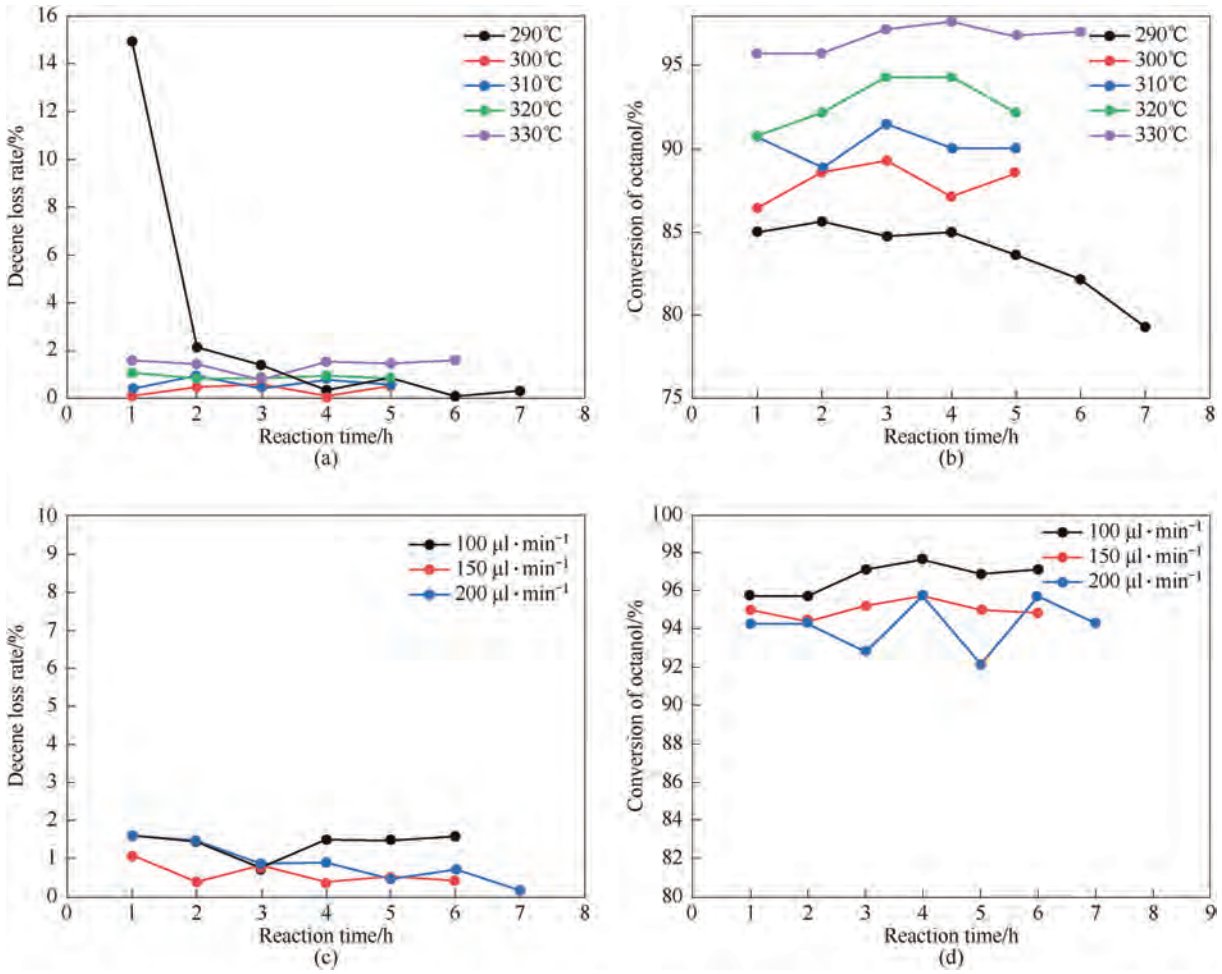

Fig. 5. (a) The isomerization loss rate of 1-decene on 1%$BaCO_3$/γ−Al_2O_3 catalyst at different reaction temperatures; (b) the dehydration conversion ratio of 1-octanol on 1%$BaCO_3$/γ−Al_2O_3 catalyst at different reaction temperatures; (c) the isomerization loss ratio of 1-decene at different injection rates at a reaction temperature of 330 °C; (d) the catalytic removal ratio of 1-octanol at different injection rates over 1%$BaCO_3$/γ−Al_2O_3 at a reaction temperature of 330 °C.

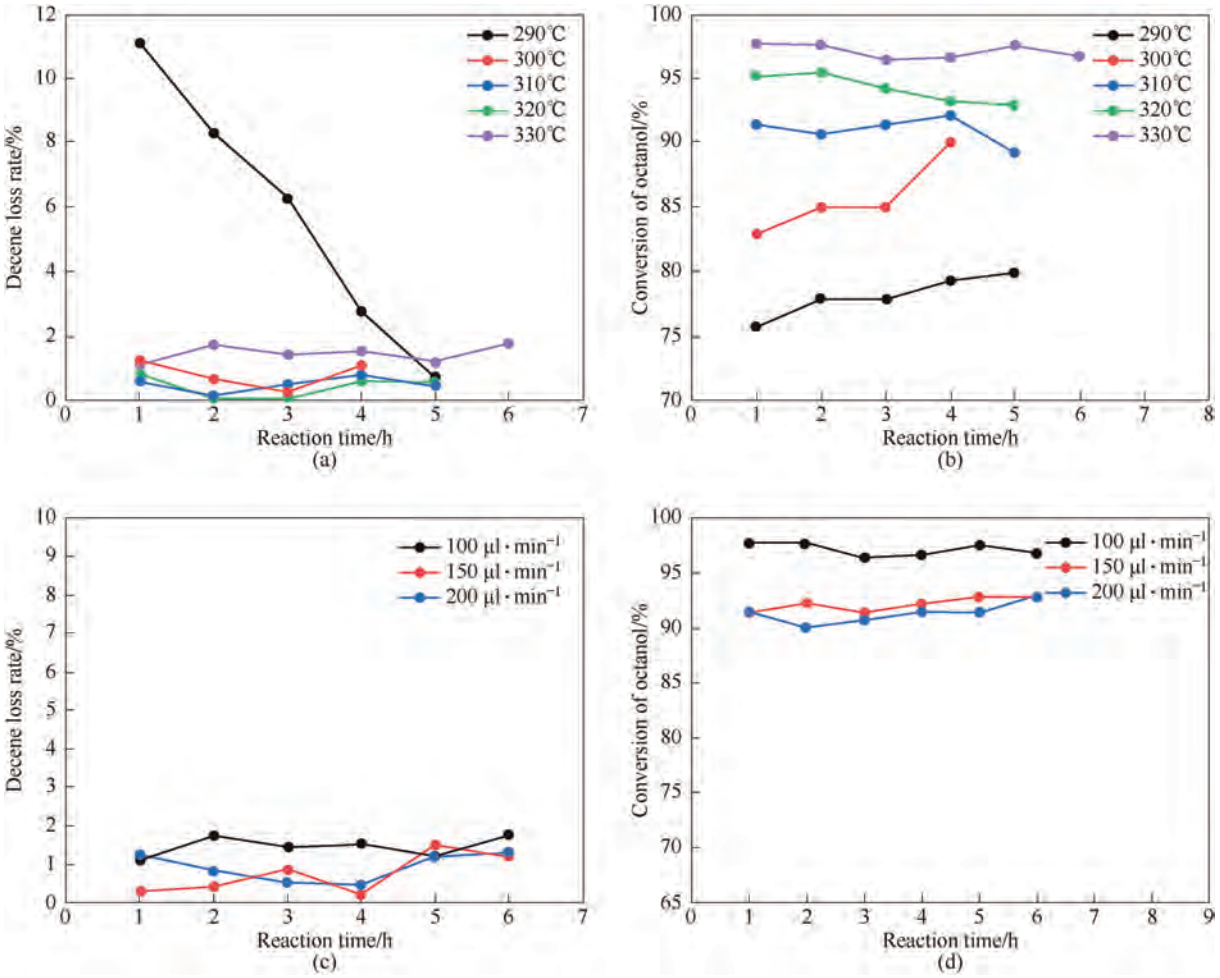

Fig. 6. (a) The isomerization loss ratio of 1-decene over 2%$BaCO_3/\gamma-Al_2O_3$ catalyst at different reaction temperatures; (b) the dehydration conversion ratio of 1-octanol on 2%$BaCO_3/\gamma-Al_2O_3$ catalyst at different reaction temperatures; (c) the isomerization loss ratio of 1-decene at different injection rates at a reaction temperature of 330 °C; (d) the catalytic removal ratio of 1-octanol at different injection rates on 2%$BaCO_3/\gamma-Al_2O_3$ at a reaction temperature of 330 °C.

3.3. Study on catalytic deoxygenation kinetics of 1-octanol

When studying the catalytic dehydration kinetics of 1-octanol, the optimized 3%$BaCO_3/\gamma$-Al_2O_3 catalyst was used as the model catalyst. The fixed-bed tube reactor was loaded with 4.6 g of 3% $BaCO_3/\gamma$-Al_2O_3, and the catalytic dehydration ratio of 1-octanol was investigated at 300, 310, 320, and 330 °C, as well as five injection rates (80, 120, 160, 200 and 240 $\mu l \cdot min^{-1}$) at each temperature. The dehydration ratio of 1-octanol was also studied upon changing the injection space speed and reaction temperature.

Table 1
The dehydration performance on 3%$BaCO_3/\gamma-Al_2O_3$ catalyst.

Reaction temperature/°C	Reaction time/h	Isomerization ratio of 1-decene/%	Dehydration ratio of 1-octanol/%
290	3	7.82	92.14
	4	4.79	90.00
	5	3.78	88.57
	6	2.78	89.28
	7	1.38	90.00
	8	0.53	90.14
	9	0.08	90.71
310	1	0.22	95.71
	2	0.89	97.14
	3	1.43	97.14
	4	1.10	97.85
	5	1.60	95.71
	6	1.03	98.57
330	1	0.98	97.14
	2	1.09	98.57
	3	0.96	98.57
	4	0.34	100.00
	5	1.28	98.57
	6	0.20	98.57

In the kinetics study, the amount of catalyst was fixed, the injection rates of C10 mixed oil were controlled by a constant-flow piston pump, and the conversion of 1-octanol at 300, 310, 320 and 330 °C and different injection rates was determined. The experimental results are shown in Tables S1–S4. W/F_m at each temperature was plotted versus the conversion X and fit according to the mathematical formula $X = A_2 + (A_1-A_2)/(1+ \exp((W/F_m-(W/F_m)_0)/d\ (W/F_m))$. The slope corresponding to each point of W/F_m was obtained from the smooth curve, *i.e.*, the reaction rate R_m at this point (Figs. S2–S5).

Each curve in Figures S6–S9 was fitted with the least-squares method, and the linear equation was obtained, respectively:

$$\ln R_m = 2.09 \ln C_m + 4.1525 \quad (1)$$

$$\ln R_m = 1.98 \ln C_m + 4.3724 \quad (2)$$

$$\ln R_m = 1.91 \ln C_m + 4.6150 \quad (3)$$

T/K	−1/T	lnK
573	−0.001745201	4.1525
583	−0.001715266	4.3724
593	−0.001686341	4.6150
603	−0.001658375	4.8121

(a)

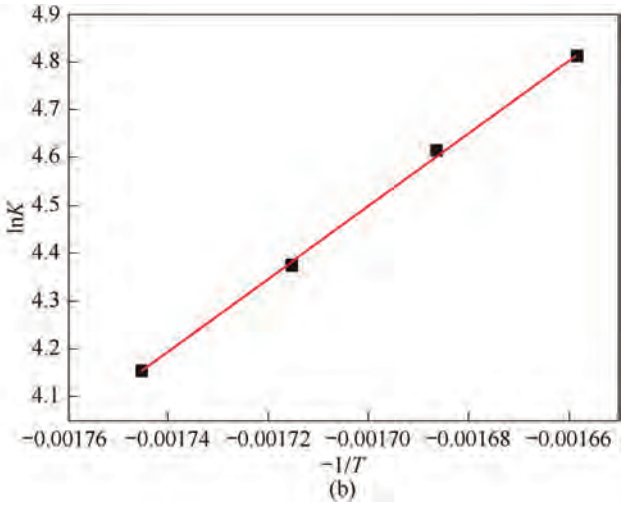

(b)

Fig. 7. (a) Reaction rate constants at different reaction temperatures. (b) The relationship between temperature and rate constant.

$$\ln R_m = 2.02 \ln C_m + 4.8121 \quad (4)$$

The coefficient in front of $\ln C_m$ is the reaction order, and the constant term behind the equation is the natural logarithm $\ln K$ of the reaction rate constant K. The reaction order remained at a constant value of 2 at 300, 310, 320 and 330 °C. Based on the above calculations, the reaction activation energy E and frequency factor k_0 were calculated, and the reaction rate constants at different temperatures are given in Fig. 7(a).

The least-squares method was used to fit Fig. 7(b), and the equation was obtained:

$$y = 0.77 \times 10^4 x + 17.55 \quad (5)$$

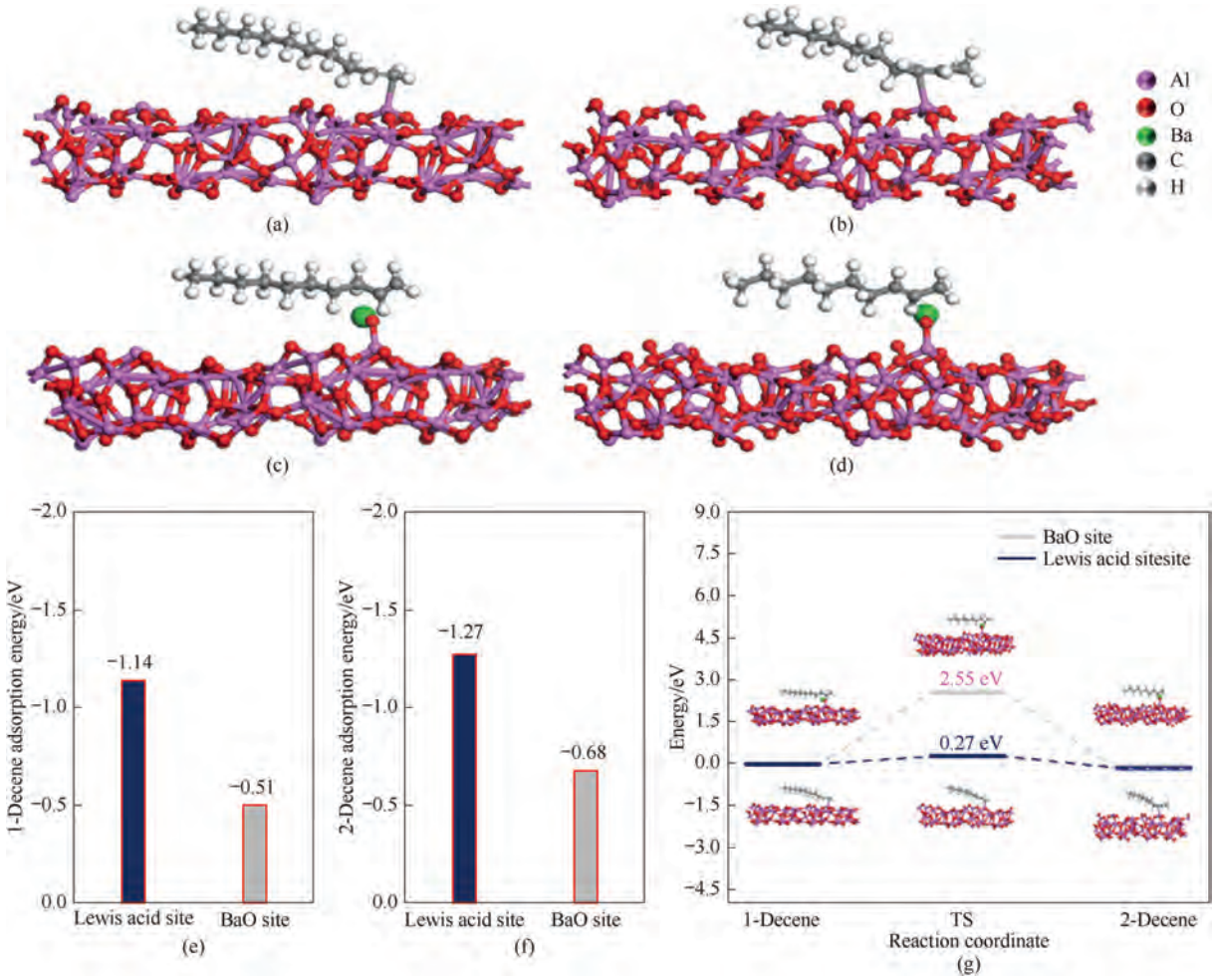

Fig. 8. Adsorption models of 1-decene (a) and 2-decene (b) on Lewis acid sites. Adsorption models of 1-decene (c) and 2-decene (d) on BaO sites. Comparisons of the adsorption energy of 1-decene (e) and 2-decene (f) on a Lewis acid site and BaO site. (g) Transition state adsorption energy of 1-decene at a Lewis acid site and BaO site.

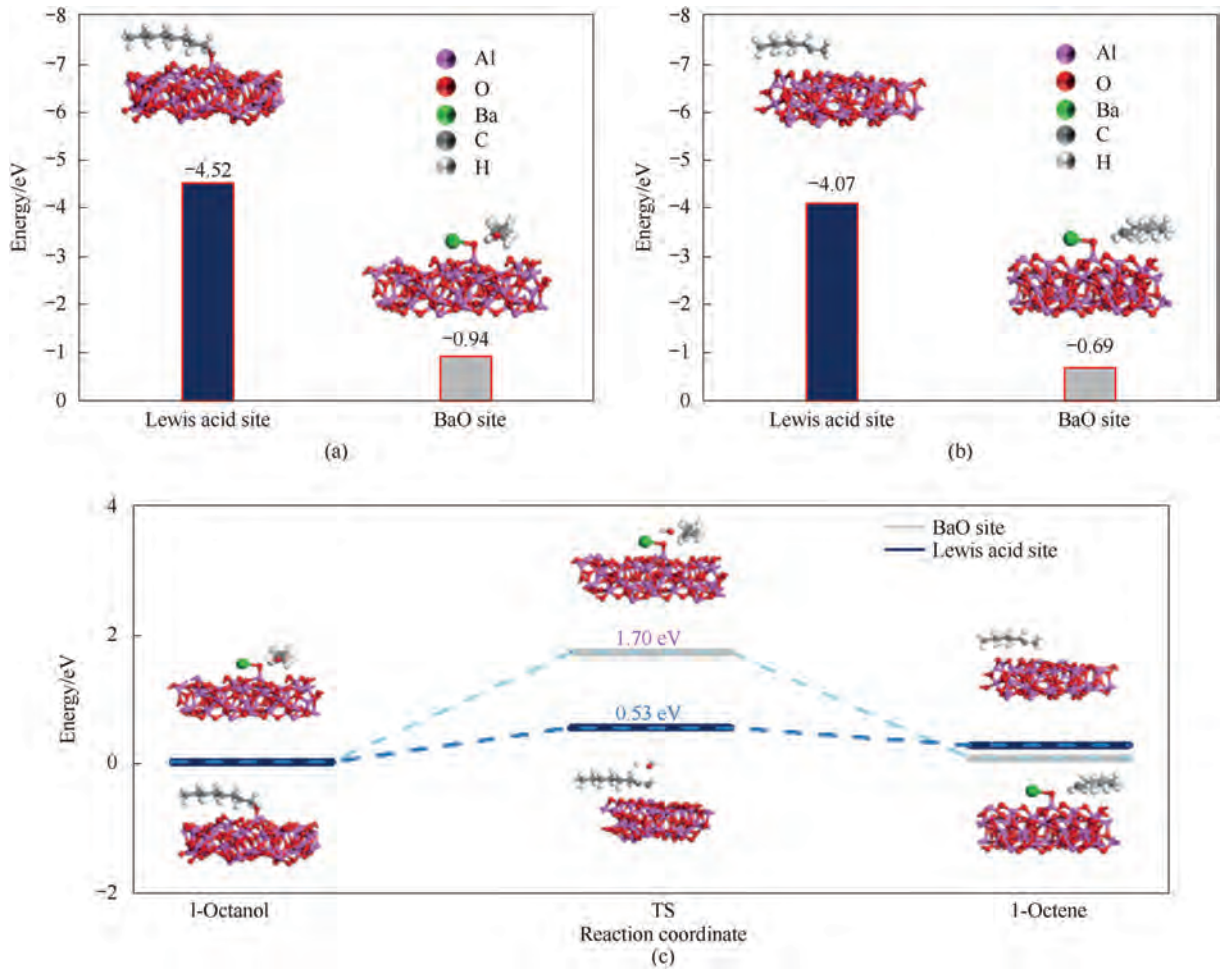

Fig. 9. (a) Adsorption model and adsorption energy of 1-octanol on Lewis acid sites and BaO sites. (b) Adsorption model and adsorption energy of 1-octene on Lewis acid sites and BaO sites. (c) Comparisons of adsorption energy of 1-octanol dehydration on Lewis acid site and BaO site.

The activation energy was:

$$E = 0.77 \times 10^4 \times 8.314/10^3 = 64.0\ \text{kJ}\cdot\text{mol}^{-1} \quad (6)$$

The frequency factor K_0 was:

$$K_0 = \exp(17.55) = 4.2 \times 10^7 \quad (7)$$

Therefore, the reaction dynamics in the range of 300–330 °C were determined to be:

$$R_{m2} = 4.2 \times 10^7 \exp(0.77 \times 10^4 /T) C_m^2 \quad (8)$$

The activation energy of the reaction was positive, indicating that 1-octanol catalytic dehydration was an overall endothermic reaction [41,42].

3.4. Isomerization mechanism of 1-decene and dehydration mechanism of 1-octanol

The Fischer-Tropsch C10 mixed oil was composed of 56.3% 1-decene, 19.63% decane, 6.14% iso-decene, and 1.4% octanol. During the catalytic dehydration of 1-octanol, the acidic sites on its surface facilitated the isomerization of 1-decene to 2-decene. In this study, the isomerization loss of 1-decene was avoided by modifying γ-Al_2O_3 with Ba alkaline sites that masked the Lewis acid sites on the surface of γ-Al_2O_3.

The adsorption energies of 1-decene and 2-decene on a Lewis acid site and BaO site were compared by theoretical calculations (Fig. 8(a)–(f)). The adsorption energy of 1-decene and 2-decene at Lewis acid sites was higher than that at BaO sites. The adsorption energy of 1-decene onto Lewis acid sites was 1.14 eV, which was higher than that of BaO sites (0.51 eV). Similarly, the adsorption energy of 2-decene onto Lewis acid sites was 1.27 eV, which was greater than that at the BaO site (0.68 eV). The results showed that 1-decene strongly adsorbed onto Lewis acid sites and easily isomerized into 2-decene. Fig. 8(g) compares the transition state adsorption energy of 1-decene onto a Lewis acid site and BaO site. The transition state energy on the BaO site was 2.55 eV, which was much higher than that on the Lewis acid site of 0.27 eV. The results showed that 1-decene had a high barrier of isomerization and did not easily isomerize into 2-decene at the basic BaO site [43,44]. However, at the Lewis acid site, 1-decene had a lower barrier of isomerization and easily isomerized into 2-decene [45]. In this study, the isomerization of 1-decene in the catalytic process can be reduced by modifying γ-Al_2O_3 with alkaline BaO.

The catalytic dehydration mechanism of 1-octanol was also investigated. As shown in Fig. 9(a), the adsorption energies of 1-octanol on Lewis acid sites and BaO sites were −4.52 eV and −0.94 eV, respectively. Fig. 9(b) shows that the adsorption energies of 1-octene on Lewis acid sites and BaO sites

were −4.07 eV and −0.69 eV, respectively. These results illustrated that the adsorption energies of 1-octanol were higher on the Lewis acid sites than on the BaO sites. Thus, 1-octanol could be easily dehydrated to 1-octene. The reaction energy barrier of the 1-octanol dehydration reaction on the Lewis acid sites was about 0.53 eV, which was lower than on the BaO sites (1.7 eV, Fig. 9(c)). The results indicated that 1-octene was more easily produced by the dehydration of 1-octanol on Lewis acid sites [38,46].

4. Conclusions

$BaCO_3/\gamma$-Al_2O_3 catalyst was prepared by the high-temperature calcination of commercial γ-Al_2O_3 modified with $BaCO_3$ with a mass fraction of 1% to 3% (mass), respectively. The catalytic performance of $BaCO_3/\gamma$-Al_2O_3 for 1-octanol dehydration in Fischer-Tropsch C10 mixture oil was evaluated in a continuous fixed-bed tubular reactor. The 3%$BaCO_3/\gamma$-Al_2O_3 catalyst showed high catalytic dehydration performance at a reaction temperature of 310 °C and a feed space velocity of 1 h^{-1}. The catalytic dehydration kinetics of 1-octanol were studied in detail, which was an endothermic reaction with an activation energy of 64 $kJ \cdot mol^{-1}$ and a reaction order of 2. The adsorption and activation of 1-decene at Lewis acid sites and basic BaO sites were studied using theoretical calculations, which showed that 1-decene was more easily isomerized into 2-decene and other internal olefins at Lewis acid sites. The 1-octanol catalytic dehydration mechanism was also investigated to provide a reference for the catalytic dehydration of Fischer-Tropsch synthetic oil.

CRediT Authorship Contribution Statement

Yongbin Shen: Writing – original draft, Investigation, Formal analysis. Qihe Ma: Validation, Methodology, Data curation. Hua Yuan: Methodology, Formal analysis, Data curation. Chuang Liu: Methodology, Investigation, Data curation. Likun Yang: Software, Resources, Methodology. Hao Huang: Validation, Funding acquisition, Formal analysis. Bowen Shi: Validation, Software, Methodology. Zhenhua Li: Visualization, Formal analysis, Conceptualization. Shunyu Liang: Methodology, Investigation, Data curation. Hu Li: Supervision, Resources, Conceptualization. Zhengping Dong: Writing – review & editing, Supervision, Conceptualization.

Declaration of Competing Interest

The authors declare that they have no known competing financial interests or personal relationships that could have appeared to influence the work reported in this paper.

Acknowledgements

This work is supported by the Scientific and technological innovation project of Ningxia Coal Industry Co., LTD, China Energy Investment (NXMY-24-36).

Supplementary Material

Supplementary data to this article can be found online at https://doi.org/10.1016/j.cjche.2025.04.009.

References

[1] K. Jeske, T. Rösler, M. Belleflamme, T. Rodenas, N. Fischer, M. Claeys, W. Leitner, A.J. Vorholt, G. Prieto, Direct conversion of syngas to higher alcohols *via* tandem integration of Fischer-Tropsch synthesis and reductive hydroformylation, *Angew. Chem., Int. Ed.* 61 (31) (2022) e202201004.
[2] J. Přech, D.R. Strossi Pedrolo, N.R. Marcilio, B. Gu, A.S. Peregudova, M. Mazur, V. V. Ordomsky, V. Valtchev, A.Y. Khodakov, Core–shell metal zeolite composite catalysts for *in situ* processing of Fischer–Tropsch hydrocarbons to gasoline type fuels, *ACS Catal.* 10 (4) (2020) 2544–2555.
[3] X.P. Fu, W.Z. Yu, C. Ma, J. Lin, S.Q. Sun, S.Q. Li, P.N. Ren, F.Y. Jia, M.Y. Li, W.W. Wang, X. Wang, C.J. Jia, K. Wu, R. Si, C.H. Yan, Supported Fe2C catalysts originated from Fe2N phase and active for Fischer-Tropsch synthesis, *Appl. Catal. B Environ.* 284 (2021) 119702.
[4] P. Wang, F.K. Chiang, J.C. Chai, A. Iulian Dugulan, J. Dong, W. Chen, R.J.P. Broos, B. Feng, Y.J. Song, Y.J. Lv, Q. Lin, R.M. Wang, I.A.W. Filot, Z.W. Men, E.J.M. Hensen, Efficient conversion of syngas to linear α-olefins by phase-pure χ-Fe_5C_2, *Nature* 635 (8037) (2024) 102–107.
[5] X.Y. Fu, J.R. Tian, M.J. Zhang, Y. Jing, Y.X. Liu, H.J. Song, Q.M. Wang, Biomimetic dehydrogenative intermolecular formal allylic amidation of branched α-olefins, *Adv. Sci.* 12 (2) (2025) 2411744.
[6] B. An, C.W. Yue, S. Liu, L.X. Sun, T.T. Sun, J.B. Liu, Y.F. Li, Radical isomerization homopolymerization of linear α-olefins to access C5, C6 or C7 polymers, *Angew. Chem., Int. Ed.* 63 (46) (2024) e202408487.
[7] C. Barzan, E. Groppo, E.A. Quadrelli, V. Monteil, S. Bordiga, Ethylene polymerization on a SiH_4-modified Phillips catalyst: detection of *in situ* produced α-olefins by operando FT-IR spectroscopy, *Phys. Chem. Chem. Phys.* 14 (7) (2012) 2239–2245.
[8] R.H. Yang, X. Chen, J.X. Ma, Y. Gao, Y.J. Wang, G.S. Luo, Direct imaging and mechanism study of C6 α-olefin adsorption on faujasite and Linde type A zeolites, *Nano Res.* 15 (6) (2022) 5322–5330.
[9] X.M. Qiu, C.T. Deng, X.Y. Cao, H.J. Gai, H.B. Song, Green and designable deep eutectic solvents for extraction separation of oxygenated compounds in Fischer-Tropsch oil products: hydrogen bond descriptors and structure–activity study, *Sep. Purif. Technol.* 330 (2024) 125540.
[10] F.Y. Zhao, R.H. Yang, J.X. Ma, Y. Gao, Y.J. Wang, G.S. Luo, Alumina microspheres for the adsorption of fatty alcohols containing oxygenates in Fischer-Tropsch synthetic oils, *Sep. Purif. Technol.* 326 (2023) 124593.
[11] Y. Xing, C.M. Masuku, L.T. Biegler, Modular gas-to-liquids process with membrane steam-methane reformer and Fischer–Tropsch reactive distillation, *AIChE. J.* 67 (12) (2021) e17467.
[12] R.H. Yang, S. Ullah, X. Chen, J.X. Ma, Y. Gao, Y.J. Wang, G.S. Luo, Selective adsorption of liquid long-chain α-olefin/paraffin on Mg-MOF-74: adsorption behavior and interaction mechanism, *Nano Res.* 16 (1) (2023) 1595–1605.
[13] Y.F. Ma, G.Y. Xu, H. Wang, Y.X. Wang, Y. Zhang, Y. Fu, Cobalt nanocluster supported on $ZrRE_nO_x$ for the selective hydrogenation of biomass derived aromatic aldehydes and ketones in water, *ACS Catal.* 8 (2) (2018) 1268–1277.
[14] Y.S. Li, H.L. Chen, J. Liu, H.B. Li, W.S. Yang, Pervaporation and vapor permeation dehydration of Fischer–Tropsch mixed-alcohols by LTA zeolite membranes, *Sep. Purif. Technol.* 57 (1) (2007) 140–146.
[15] R.R. Zhang, Y. Huang, K.T. Zheng, C.J. Xu, Design and control of fraction cutting for the separation of mixed alcohols from the Fischer–Tropsch aqueous byproducts, *Chin. J. Chem. Eng.* 50 (2022) 143–154.
[16] R.J.J. Nel, A. de Klerk, Dehydration of C_5–C_{12} linear 1-alcohols over η-alumina to fuel ethers, *Ind. Eng. Chem. Res.* 48 (11) (2009) 5230–5238.
[17] A. de Klerk, Contributions of burtron H. Davis to Fischer–Tropsch refining catalysis: dehydration as applied to processes for 1-octene production, *Top. Catal.* 57 (6) (2014) 715–722.
[18] J.H. Lee, W.J. Kim, D. Park, Y. Jo, J.H. Baik, Y.W. Suh, Zirconia-incorporated yttria with a Lewis pair of acid–base surface sites for chemoselective dehydration of alcohols into alpha olefins, *Appl. Catal. Gen.* 678 (2024) 119707.
[19] D.J. McClelland, B.X. Wang, W.T. Cordell, Y.R. Cortes-Peña, E.B. Gilcher, L.F. Zhang, J.S. Guest, B.F. Pfleger, G.W. Huber, J.A. Dumesic, Renewable linear alpha-olefins by base-catalyzed dehydration of biologically-derived fatty alcohols, *Green Chem.* 23 (12) (2021) 4338–4354.
[20] D. Hua, R.K. Rai, Y. Zhang, T.S. Chung, Aldehyde functionalized graphene oxide frameworks as robust membrane materials for pervaporative alcohol dehydration, *Chem. Eng. Sci.* 161 (2017) 341–349.
[21] Y.M. Wang, F. Lorenzini, M. Rebros, G.C. Saunders, A.C. Marr, Combining bio- and chemo-catalysis for the conversion of bio-renewable alcohols: homogeneous iridium catalysed hydrogen transfer initiated dehydration of 1, 3-propanediol to aldehydes, *Green Chem.* 18 (6) (2016) 1751–1761.
[22] B. Tran, S.T. Milner, M.J. Janik, Kinetics of acid-catalyzed dehydration of alcohols in mixed solvent modeled by multiscale DFT/MD, *ACS Catal.* 12 (21) (2022) 13193–13206.
[23] J. Ballesteros-Soberanas, L.D. Ellis, J.W. Medlin, Effects of phosphonic acid monolayers on the dehydration mechanism of aliphatic alcohols on TiO_2, *ACS Catal.* 9 (9) (2019) 7808–7816.
[24] N. Pfriem, Y. Liu, F. Zahn, H. Shi, G.L. Haller, J.A. Lercher, Impact of the local concentration of hydronium ions at tungstate surfaces for acid-catalyzed alcohol dehydration, *J. Am. Chem. Soc.* 143 (48) (2021) 20133–20143.
[25] I. Coleto, R. Roldán, C. Jiménez-Sanchidrián, J.P. Gómez, F.J. Romero-Salguero, Valorization of α-olefins: double bond shift and skeletal isomerization of 1-pentene and 1-hexene on zirconia-based catalysts, *Catal. Today* 149 (3–4) (2010) 275–280.
[26] D. Nguyen, S.G. Wang, L.C. Grabow, E. Harth, Deciphering the olefin isomerization-polymerization paradox of palladium(II) diimine catalysts:

discovery of simultaneous and independent pathways of olefin isomerization and living polymerization, *J. Am. Chem. Soc.* 145 (17) (2023) 9755–9770.
[27] A.C. Jerdy, L. Trevisi, M. Monwar, M.Á. González-Borja, R. Abbott, L. Lobban, S. Crossley, Deconvoluting the roles of polyolefin branching and unsaturation on depolymerization reactions over acid catalysts, *Appl. Catal. B Environ.* 337 (2023) 122986.
[28] A. Kunamalla, S.K. Maity, Production of green jet fuel from furanics *via* hydroxyalkylation-alkylation over mesoporous MoO_3-ZrO_2 and hydrodeoxygenation over Co/γ-Al_2O_3: role of calcination temperature and MoO_3 content in MoO_3-ZrO_2, *Fuel* 332 (2023) 125977.
[29] G. Kresse, D. Joubert, From ultrasoft pseudopotentials to the projector augmented-wave method, *Phys. Rev. B* 59 (3) (1999) 1758–1775.
[30] G. Kresse, J. Furthmüller, Efficient iterative schemes for *ab initio* total-energy calculations using a plane-wave basis set, *Phys. Rev. B Condens. Matter* 54 (16) (1996) 11169–11186.
[31] J.P. Perdew, K. Burke, M. Ernzerhof, Generalized gradient approximation made simple, *Phys. Rev. Lett.* 77 (18) (1996) 3865–3868.
[32] S.Y. Ahn, W.J. Na, K.J. Kim, B.J. Kim, S.J. Ryu, H.S. Roh, H.K. Park, Upgrading the catalytic activity recovery capacity of a Ni–Mo/γ-Al_2O_3 catalyst *via* a modified remanufacturing process for residue hydrodesulfurization: effect of acid leaching conditions and process sequence, *Catal. Today* 425 (2024) 114335.
[33] F. Yan, J.G. Jiang, N. Liu, Y.C. Gao, Y. Meng, K.M. Li, X.J. Chen, Green synthesis of mesoporous γ-Al_2O_3 from coal fly ash with simultaneous *on-site* utilization of CO_2, *J. Hazard. Mater.* 359 (2018) 535–543.
[34] A. Akbarzadeh, M. Ahmadlouydarab, A. Niaei, Capabilities of α-Al_2O_3, γ-Al_2O_3, and bentonite dry powders used in flat plate solar collector for thermal energy storage, *Renew. Energy* 173 (2021) 704–720.
[35] Y.J. Sun, P. Li, H.L. Zheng, C. Zhao, X.F. Xiao, Y.H. Xu, W.Q. Sun, H.F. Wu, M.J. Ren, Electrochemical treatment of chloramphenicol using Ti-Sn/γ-Al_2O_3 particle electrodes with a three-dimensional reactor, *Chem. Eng. J.* 308 (2017) 1233–1242.
[36] T.W. Zhang, Y.C. Jin, H.N. Xiao, Efficient production of 5-hydroxymethylfurfural from glucose over sulfonated carbon/γ-Al_2O_3 composite, *Fuel* 381 (2025) 133414.
[37] Y.E. Kim, H.B. Im, U.H. Jung, J.C. Park, M.H. Youn, H.D. Jeong, D.W. Lee, G.B. Rhim, D.H. Chun, K.B. Lee, K.Y. Koo, Production of linear α-olefin 1-octene *via* dehydration of 1-octanol over Al_2O_3 catalyst, *Fuel* 256 (2019) 115957.
[38] D.W. Lee, M.H. Jin, J.H. Park, Y.J. Lee, Y.C. Choi, Y.E. Kim, K.Y. Koo, J.C. Park, M. H. Youn, D.H. Chun, Production of linear alpha olefin 1-octene through 1-octanol dehydration in packed-bed membrane reactors with large mesoporous membranes (PMRL) for remarkable improvement in 1-octanol conversion and 1-octene yield, *Fuel* 333 (2023) 126367.
[39] H. Zou, T. Pan, Y.W. Shi, Y.W. Cheng, L.J. Wang, Y. Zhang, X. Li, Light olefin production by catalytic co-cracking of Fischer–Tropsch distillate with methanol and the reaction kinetics investigation, *Chin. J. Chem. Eng.* 28 (1) (2020) 143–151.
[40] R.M. Malek Abbaslou, J.S. Soltan Mohammadzadeh, A.K. Dalai, Review on Fischer–Tropsch synthesis in supercritical media, *Fuel Process. Technol.* 90 (7–8) (2009) 849–856.
[41] M.J. Hidajat, G.N. Yun, D.W. Hwang, Numerical and statistical determinations of the controlling factors in biomass-derived alcohol dehydration over La-incorporated γ-Al_2O_3 catalysts, *Chem. Eng. J.* 473 (2023) 145376.
[42] Y.E. Kim, U. Jung, D. Song, H.B. Im, J.C. Park, M.H. Youn, H.D. Jeong, G.B. Rhim, D. H. Chun, D.W. Lee, K.B. Lee, K.Y. Koo, Effect of Ba impregnation on Al_2O_3 catalyst for 1-octene production by 1-octanol dehydration, *Fuel* 281 (2020) 118791.
[43] F.Q. Gong, N.W. Liu, L. Shi, X. Meng, Application of alkali-treated MCM-22 zeolite in catalytic 1-decene oligomerization reaction, *Fuel* 344 (2023) 128104.
[44] K.E. Kawamura, A.S. Chang, D.J. Martin, H.M. Smith, P.T. Morris, A.K. Cook, Modular Ni(0)/silane catalytic system for the isomerization of alkenes, *Organometallics* 41 (4) (2022) 486–496.
[45] J. Yan, P. Wang, T. Yan, C.C. Ao, L.D. Zhang, L.L. Lei, A theoretical calculation and kinetic modeling analysis of H-abstraction from 1-octene for subsequent isomerization and β-dissociation, *Int. J. Hydrogen Energy* 55 (2024) 1028–1036.
[46] Y.E. Kim, U. Jung, D. Song, H.B. Im, T.H. Lee, D.H. Chun, M.H. Youn, K.B. Lee, K. Y. Koo, Dual-bed catalytic system comprising Al_2O_3 and Ba/Al_2O_3 with enhanced 1-octene productivity in 1-octanol dehydration for linear α-olefin production, *J. Ind. Eng. Chem.* 119 (2023) 376–385.